

Configurational control of photon emission from a molecular dimer

Maximilian Kögler,* Nicolas Néel, and Jörg Kröger*

Institut für Physik, Technische Universität Ilmenau, D-98693 Ilmenau, Germany

E-mail: max.koegler@tu-ilmenau.de; joerg.kroeger@tu-ilmenau.de

Abstract

Tin-phthalocyanine molecules adsorbed on a NaCl ultrathin film on Au(111) exhibit electrofluorescence excited by a current across a scanning tunneling microscope junction. Exploring the dependence of the molecular monomer photon yield on the injected current evidences the one-electron excitation process underlying the neutral-exciton luminescence. Photon spectra of the monomer exhibit vibrational progression and hot luminescence, while the dimer electrofluorescence spectroscopic fine structure results from the coupling of the adjacent optical transition dipoles. The photon yield of the dimer is significantly altered upon changing the configurational state of one of the two molecules. In one of the bistable configurations light emission is amplified compared to the monomer, and it is reduced in the other.

Keywords: electroluminescence, scanning tunneling microscope, single molecule, exciton, coherent dipole-dipole coupling

Research devoted to quantum photon emitters, for instance semiconductor quantum dots,¹⁻³ atoms,^{4,5} color centers,⁶⁻⁸ and molecules,⁹⁻¹⁴ is stimulated by the rapid progression of quantum-technological applications, e. g., cryptology and information processing,¹⁵⁻²¹ quantum computing,²² the simulation of quantum mechanics,²³ quantum sensing²⁴ and metrology.²⁵ Likewise, fundamental aspects, for example the coupling of the exciton underlying

the photon emission to the optical cavity for enhanced photon yield²⁶⁻²⁹ or the radiative correlation of a group of quantum emitters giving rise to the coherent superposition of the individual emitter states,^{26,30-41} belong to the highly topical developments in the field.

The scanning tunneling microscope (STM) plays a particularly appealing role in exploring quantum optical effects for several reasons. To thoroughly study structural, electronic, and optical properties of quantum emitters, such as single molecules, the atomic scale, which is the resolution realm of an STM,⁴² must be accessible. In addition, the atom-by-atom manipulation of matter by using the STM tip^{43,44} is advantageous to fabricate artificial assemblies of atomic or molecular emitters. Moreover, the spectroscopy of STM-induced light emission (STML) was demonstrated for molecular crystals⁴⁵ and single molecules,⁴⁶ which opened the avenue to exploring quantum optics at the single-atom and single-molecule level.^{47,48}

Of particular interest to the work presented here is the amplification of photon emission reported for Zn-phthalocyanine (Zn-Pc) dimers³⁷ and for chains of up to twelve Zn-Pc molecules⁴¹ on NaCl-covered Ag(100) compared to the photon yield of the monomer. In both cases, the coherent dipole-dipole coupling between the molecules in close proximity induced a collective state underlying the observed photon yield enhancement. The report presented here was mainly motivated by identifying a molecular assembly that allows the external control of light amplification at the single-molecule level. The use of Sn-Pc monomers and dimers on NaCl-covered Au(111) proved successful to this end. The Sn-Pc molecule offers the reversible transfer of its central Sn atom through the macrocycle resulting in two bistable configurations with the Sn atom above (Sn-Pc-*u*) and beneath (Sn-Pc-*d*) the molecular backbone,⁴⁹ which are achieved by charge injection from the STM tip. An Sn-Pc dimer with the *uu* combination of configurations gives rise to a larger photon yield than observed from the Sn-Pc-*u* monomer, while light emission of the *ud* combination is nearly suppressed. The key finding is therefore the reversible switch between a bright and a dark optical state of an Sn-Pc dimer. In addition, since STML of Sn-Pc is reported here for the first time, the present work

thoroughly characterizes the electroluminescence spectra of the monomer and the dimer. The photon emission is due to a neutral molecular exciton and represents a one-electron excitation. While the STML spectrum of an Sn-Pc-*u* monomer exhibits fine structure due to vibrational progression and hot luminescence, the Sn-Pc-*u* dimer gives rise to emission characteristics that are compatible with coupled molecular transition dipole moments.

Figure 1a illustrates the basic STM junction geometry of the STML experiments comprising an Au-covered Ag tip and an Sn-Pc molecule residing atop an ultrathin NaCl film on Au(111) (details are presented in the Supporting Information, Figure S1). Three and four atomic layers of NaCl with apparent heights (measured at 1.9 V) of about 430 pm and 580 pm, respectively, resulted from the preparation protocol (Methods), which is in agreement with previous work.⁵⁰ Unless otherwise stated, the presented data were obtained on 4-layer thin NaCl islands.

A typical STM image of a single Sn-Pc-*u* is presented in Figure 1b. The strongest contribution to the image is due to the Sn atom, which in this molecular configuration points toward the tip. The Sn-associated protrusion exhibits a shallow central depression, which is assigned to the orbital texture of the molecule, as reported earlier.^{49,51} The outer regions of the four cloverlike isoindole moieties appear as two split lobes each, which was observed for Sn-Pc on molecular spacers, too, and associated with the charge density pattern of the lowest unoccupied molecular orbital (LUMO).⁴⁹

Figure 1c depicts the photon yield spectrum of Sn-Pc-*u* in a wide range of photon energies. Details of optical data processing are described in the Supporting Information (Figure S2). The monomer spectrum was obtained by parking the tip above one of the split lobes (dot in Figure 1b) at positive voltage. Elevated negative voltages turned out to move Sn-Pc-*u* and, thus, were not suitable for STML. The emission peak at 1.75 eV is consistent with the previously determined absorbance maximum of Sn-Pc in a benzene solution of 1.78 eV.^{52,53} The discrepancy in emission and absorbance maxima is likely due to the different dielectric environments in the two cases. In accordance with theoretical studies,⁵⁴ the Sn-Pc absorption

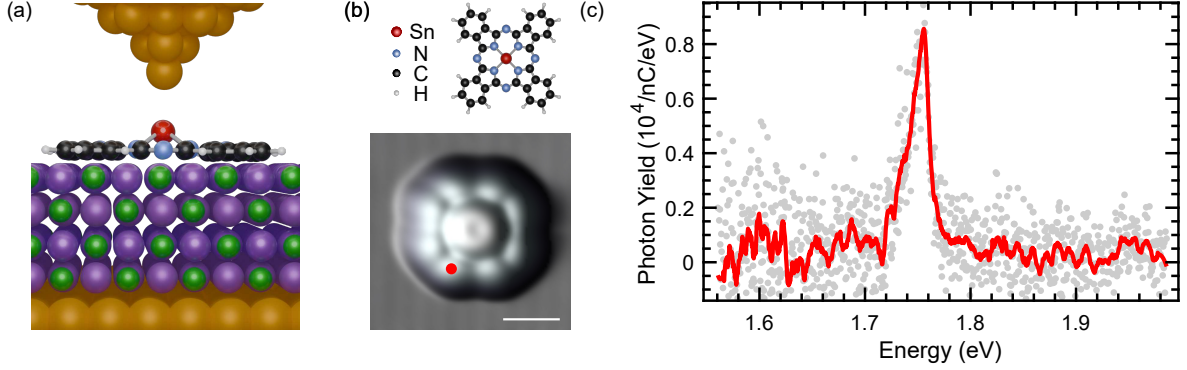


Figure 1: Electroluminescence spectroscopy of an Sn-Pc-*u* monomer. (a) Sketch of the junction geometry including an Au-covered tip and the top surface layer (yellow) of Au(111) as well as a single Sn-Pc-*u* molecule (H: white, C: black, N: blue, Sn: red) residing atop 4 atomic NaCl (Na: green, Cl: violet) layers. (b) Top: top view of the relaxed vacuum structure of Sn-Pc. Bottom: constant-current STM image of a single Sn-Pc-*u* molecule on NaCl (sample voltage: 1.9 V, current: 20 pA, the gray scale covers apparent heights ranging from 0 pm (dark) to 695 pm (bright)). The scale bar indicates 1 nm. (c) Wide range STML spectrum (dots) of Sn-Pc-*u* acquired at 2.5 V, 80 pA for 180s above the position indicated by the dot in (b). The solid line represents smoothed data.

was assigned to the Q-band, which mainly involves the electronic excitation from the highest occupied molecular orbital (HOMO) to the LUMO. Therefore, the Sn-Pc-*u* photon emission line visible in Figure 1c can reasonably be associated with the neutral Q-exciton of the molecule. Electrofluorescence spectra of the Sn-Pc-*d* monomer were hampered due to its unintentional conversion to Sn-Pc-*u* at the tunneling gap parameters required for a decent photon signal.

In Figure 2, electrofluorescence spectroscopy with enhanced optical resolution of Sn-Pc-*u* monomers and dimers is analyzed in detail. The emission spectrum of a single Sn-Pc-*u* molecule is shown in Figure 2a. Besides the principal transition from the electronic excited (S_1) to the electronic ground (S_0) state with energy $E_{00} = 1.758$ eV), spectroscopic fine structure is observed both at energies below (E_{i0}) and above (E_{0i}) the $S_1 \rightarrow S_0$ transition (dashed lines). While the emission features for $E_{i0} < E_{00}$ are attributed to vibrational progression, the group of emission lines with $E_{0i} > E_{00}$ is assigned to hot luminescence. The indices in $E_{\nu\nu'}$ denote the vibrational states of S_0 (ν) and S_1 (ν') with $\nu = 0$ ($\nu' = 0$)

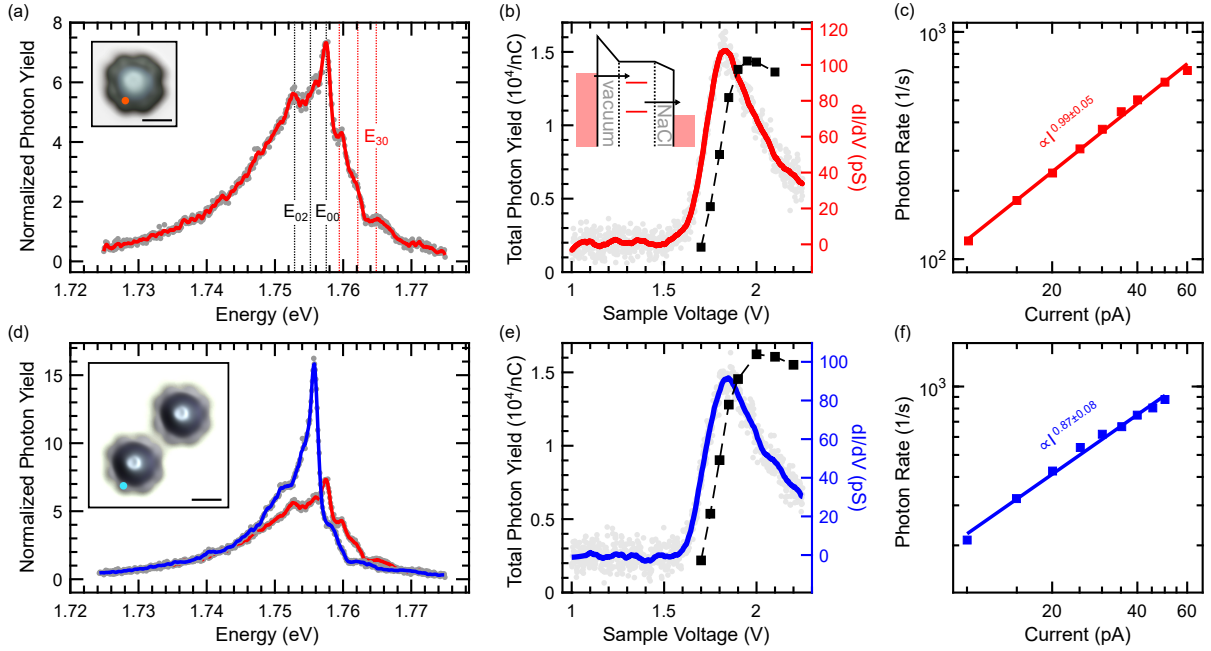


Figure 2: Photon emission characteristics of Sn-Pc-*u* monomers and dimers. (a) Spectral photon yield of Sn-Pc-*u* recorded at 1.9 V, 50 pA for 180 s. The data are normalized by the spectrum of the tip-induced plasmon acquired above the bare NaCl island with the same tip. Inset: constant-height STM image of Sn-Pc-*u* (1.9 V, the gray scale encodes currents ranging from 10 pA (dark) to 100 pA (bright), scale bar: 1 nm). The dot indicates the tip position for luminescence spectroscopy. (b) Constant-height spectrum of dI/dV (dots) recorded above the same position as the light spectrum (feedback loop parameters: 1.9 V, 20 pA). The solid line represents smoothed data. Squares depict the integrated spectral photon yield of (a) with the dashed line as a guide to the eye. Inset: illustration of alignment of tip and sample electron chemical potentials with molecular frontier orbitals for the resonant excitation of the molecule by tunneling electrons. Arrows indicate tunneling of electrons from the tip across the vacuum barrier to the LUMO and from the HOMO across the NaCl barrier to the sample. (c) Evolution of photon rate (squares) with the junction current at 1.9 V. The solid line is a power law fit to the data. (d)–(f) As (a)–(c) for an Sn-Pc-*u* dimer. In (d), the acquisition time for the dimer spectrum is 240 s and a monomer spectrum (red) recorded with the same tip as the dimer spectrum is added for comparison. Inset to (d): constant-height STM image of an artificially assembled Sn-Pc-*u* dimer (1.9 V, the gray scale encodes currents ranging from 10 pA (dark) to 75 pA (bright), scale bar: 1 nm).

reflecting the vibrational ground state of S_0 (S_1). A fit to the data using a superposition of equidistant Lorentzian line shapes (Supporting Information, Figure S3) performed separately for $E < E_{00}$ and $E > E_{00}$ reproduces the emission spectrum and yields vibrational energy quanta of 2.5 meV and 3.0 meV for S_0 and S_1 , respectively. Such low-energy vibrational excitations can be assigned to librations, which represent frustrated rotations of the molecule and were observed for other phthalocyanine molecules, too.⁵⁵

Figure 2b compares the LUMO-related dI/dV signature (dots) with the total photon yield (squares) of the Sn-Pc-*u* monomer, which represents the integrated spectral photon yield (total photon yield) in the energy interval $1.7 \text{ eV} \leq E \leq 1.8 \text{ eV}$. The LUMO-associated signal increases with increasing voltage and reaches its maximum at 1.8 V. The total photon yield follows the same trend, albeit shifted by $\approx 0.2 \text{ V}$ to higher voltages. Consequently, for Sn-Pc-*u* photon emission the alignment of the tip electron chemical potential with the LUMO is required (inset to Figure 2b). Moreover, assuming the HOMO alignment with the electron chemical potential of the sample, the Q-exciton of Sn-Pc-*u* is formed by an electron attached to the LUMO and a hole transferred to the HOMO, as observed for electroluminescence of a variety of molecules.^{37,46,56-59} This assumption is in line with dI/dV spectroscopy of the molecular frontier orbitals (Supporting Information, Figure S4) after considering the voltage drop across the NaCl film and the deviation of the sought-after LUMO (HOMO) from the measured negative (positive) ion resonance.⁶⁰ The attachment of one electron and one hole to the frontier orbital levels also reflects the photon emission of the molecule in its neutral state. By exploring the current dependence of the photon rate, which is the product of the total photon yield and the current a power law behavior I^α with $\alpha = 0.99 \pm 0.05$ is found (Figure 2c). The near-unity exponent evidences a one-electron process in the electron-to-photon conversion.

Dimers were fabricated by pushing one monomer with the tip to a second Sn-Pc-*u* molecule, which was achieved with feedback loop parameters of -3.1 V and 20 pA and the tip placed atop an isoindole group of the pushed monomer (Supporting Information, Figure

S5). Figure 2d shows the electrofluorescence spectrum of an Sn-Pc dimer in the uu configuration, where the dimer partners are separated by 2.3 nm (measured between the Sn centers, inset to Figure 2d). The spectral centroid is redshifted by ≈ 2 meV with respect to the monomer spectrum and the extent of the redshift increases with decreasing intermolecular separation (Supporting Information, Figure S6). In addition, the maximum photon yield of the dimer exceeds the one of the monomer by nearly a factor of 2, and at the same time the overall width of the spectrum is smaller than observed for the monomer. Furthermore, the spectroscopic fine structure visible in the uu dimer spectrum is of different nature and will be discussed below. The variation of the dI/dV signature of the LUMO is imprinted on the voltage evolution of the total photon yield (Figure 2e), in a similar manner as observed for the monomer. Consequently, alignment of the electrode chemical potentials with the frontier orbitals is required for the dimer photon emission, which also occurs in the neutral state of the uu hybrid. A power law behavior of the photon rate with the tunneling current (Figure 2f) is likewise observed with an exponent of $\alpha = 0.87 \pm 0.08$ that within the uncertainty margins is similar to the exponent observed for the monomer.

While the voltage dependence of the total photon yield and the current dependence of the photon rate are similar for the monomer and dimer electroluminescence, the spatial dependence of monomer and dimer light emission is markedly different (Figure 3). The explanation of these differences includes the revelation of the different nature of the dimer luminescence fine structure. To explore the spatial emission characteristics of the Sn-Pc- u monomer (Figure 3a) the tip was parked above each of the 8 lobes. At each lobe, the line shapes of the monomer spectra are similar and are dominated by the emission peak due to the $S_1 \rightarrow S_0$ transition (gray stripe in Figure 3a). Its position changes by at most 1 meV. These changes may be due to the photonic Lamb shift²⁶ caused by the coupling of the nanocavity plasmon and the molecular transition dipoles. The spatial magnitude of the photon yield shows a marked variation depending on the lobe, which does not reflect the C_{2v} symmetry of the molecule. While a clear-cut rationale for this observation is missing to date, the exact

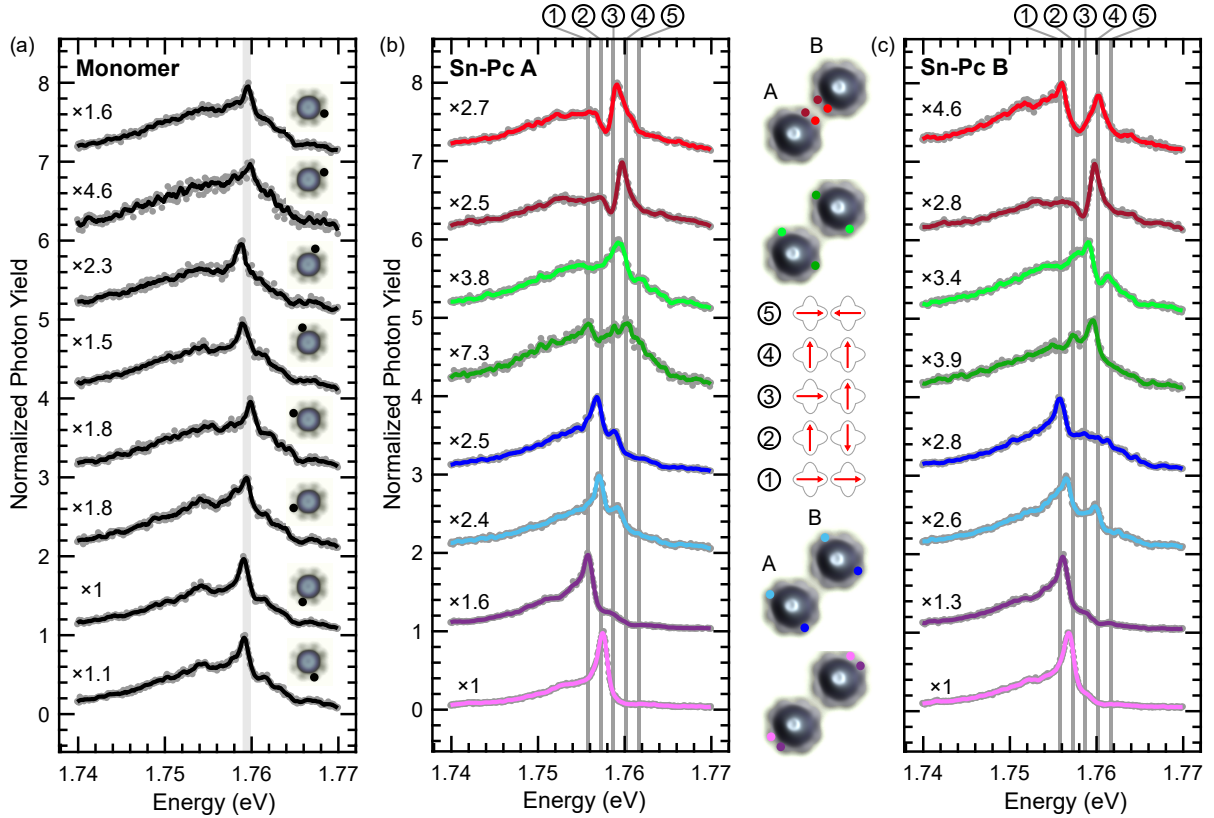


Figure 3: Spatially resolved electroluminescence spectra of the Sn-Pc-*u* monomer and *uu* dimer. (a) Site dependence of the normalized monomer spectral photon yield (1.9 V, 50 pA, 120 s). The position of spectroscopy is marked by the dot in the constant-height STM images (1.9 V, 2.3 nm \times 2.3 nm, the gray scale encodes currents ranging from 2 pA (dark) to 30 pA (bright)). The vertical stripe has a width of 1 meV and marks the $S_1 \rightarrow S_0$ transition in all spectra. (b),(c) Site dependence of the normalized *uu* dimer spectral photon yield (1.9 V, 50 pA, 120 s) atop the indicated (dots) positions. The position of spectroscopy is marked by the dot in the constant-height STM images (1.9 V, 5 nm \times 5 nm, the gray scale encodes currents ranging from 10 pA (dark) to 75 pA (bright)), where the individual monomer molecules of the dimer are labeled *A* and *B*. The vertical lines 1–5 indicate the dipole-coupled exciton states (see illustrations between (b) and (c)) underlying the fine structure. The spectra in (a)–(c) are normalized to their corresponding maximum and vertically offset.

lobe position atop the atomic NaCl lattice may be important. Indeed, extrapolating the atomically resolved NaCl lattice beneath the Sn-Pc-*u* monomer reveals that the isoindole moieties do not share equivalent adsorption sites (Supporting Information, Figure S7).

In striking contrast to the observations for the monomer, the dimer spectral photon yield exhibits pronounced peaks in an energy interval of 6 meV (vertical lines) whose signal strength varies markedly depending on the position of spectroscopy (Figures 3b,c). In total, 5 major transition peaks can be identified. At the same time, the spatially resolved dI/dV spectra of the dimer (Figure 2e and Supporting Information, Figure S4) are similar to the monomer data, which reflects the spatially unaltered electronic level alignment for photon emission. Therefore, the *uu* dimer luminescence fine structure is rationalized in terms of the coherent intermolecular transition dipole coupling (TDC), which was previously reported for Zn-Pc oligomers.³⁷ Due to TDC, the molecular dimer exhibits two single-exciton states for each of the two transition dipole moments with wave functions $\Psi^\pm = (\psi_{1e}\psi_{2g} \pm \psi_{1g}\psi_{2e})/\sqrt{2}$ where ψ_{kg} , ψ_{ke} denote the ground (g) and excited (e) exciton states of the monomer $k = 1, 2$. The associated dimer exciton energies are $E^\pm = E_{00} + \Delta \pm |J|$ with E_{00} the monomer exciton energy, Δ the van der Waals energy difference between the dimer ground and excited states, and $|J|$ the coupling strength between the monomer transition dipoles $\boldsymbol{\mu}_k$. In the point-dipole approximation,⁶¹ $J = J_0 [\boldsymbol{\mu}_1 \cdot \boldsymbol{\mu}_2 - 3(\boldsymbol{\mu}_1 \cdot \hat{\boldsymbol{r}})(\boldsymbol{\mu}_2 \cdot \hat{\boldsymbol{r}})]$ with $J_0 = 1/(4\pi\epsilon_0 r^3)$, ϵ_0 the vacuum permittivity, r the center-to-center distance of the monomers, and $\hat{\boldsymbol{r}} = \boldsymbol{r}/r$ the associated unit distance vector. For calculating J , different orientations of $\boldsymbol{\mu}_k$ are considered. While for planar Zn-Pc the transition dipole moments are oriented parallel to the molecular plane,³⁷ the three-dimensional shuttlecock geometry of Sn-Pc (Figure 1a)^{49,54,62} possibly gives rise to an out-of-plane orientation of $\boldsymbol{\mu}_k$. However, the monomer exciton involves the HOMO and LUMO, which are mainly confined to the almost planar isoindole moieties of Sn-Pc.⁵²⁻⁵⁴ Therefore, planar transition dipoles are assumed for Sn-Pc as well. Defining then directions of $\boldsymbol{\mu}_k$ as \uparrow, \downarrow perpendicular to $\hat{\boldsymbol{r}}$ and as \leftarrow, \rightarrow parallel to $\hat{\boldsymbol{r}}$, 5 TDC modes (Figures 3b,c) $\rightarrow\rightarrow$ (1), $\uparrow\downarrow$ (2), $\rightarrow\uparrow$ (3), $\uparrow\uparrow$ (4), $\rightarrow\leftarrow$ (5) with energies $-2\mu^2 J_0, -\mu^2 J_0, 0, \mu^2 J_0, 2\mu^2 J_0$, respectively,

are expected for $\mu = |\mu_1| = |\mu_2|$. With these assumptions, $\mu^2 J_0$ can be determined from the experimental data as the average distance between adjacent spectral photon yield peaks (vertical lines in Figures 3b,c), which results in (1.5 ± 0.2) meV and which is comparable with the smallest splitting reported for Zn-Pc $((3.0 \pm 1.5)$ meV).³⁷ In a few spectra, a broad spectral photon yield peak was found between two energies defined by neighboring vertical lines, which is likely caused by the superposition of two adjacent peaks.

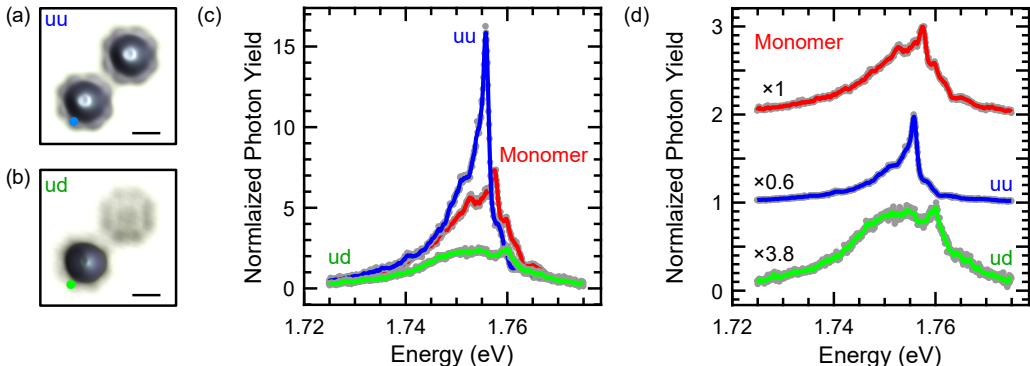


Figure 4: Electrofluorescence of *uu* and *ud* Sn-Pc dimers. (a),(b) Constant-height STM image of a *uu* (a) and a *ud* (b) dimer (1.9 V, the gray scale encodes currents from (a) 10 pA, (b) 2 pA (dark) to (a) 75 pA, (b) 25 pA (bright), scale bar: 1 nm). (c) Normalized spectral photon yield of an Sn-Pc-*u* monomer and Sn-Pc dimers in the *uu* and *ud* configuration (1.9 V, 50 pA, 240 s). All spectra were recorded with the same tip above the positions indicated by the dots in (a),(b). They are normalized by the tip plasmon luminescence spectrum atop bare NaCl. (d) Same as (c) with the spectra normalized by their respective maximum and vertically offset.

Before addressing the amplification of the photon yield in the TDC model, the electroluminescence of the dimer in the *ud* configuration is discussed. Stimulated by electron injection, the Sn atom can reversibly be transferred across the molecular macrocycle, as originally demonstrated for molecular decoupling layers⁴⁹ and later for various substrates.^{63–65} Placing the tip above the central Sn atom of an Sn-Pc-*u* molecule at negative voltage leads to the $u \rightarrow d$ conversion, while the $d \rightarrow u$ conversion is achieved for positive voltage (Supporting Information, Figure S5). Unlike for Sn-Pc-*u*, the isoindole groups protrude towards the tip for Sn-Pc-*d*, and the center is imaged as a depression. Figure 4 compares electro-

luminescence spectroscopy for an Sn-Pc dimer in the uu (Figure 4a) and in the ud (Figure 4b) configuration. In order to avoid the unintentional $d \rightarrow u$ conversion at the elevated positive voltages required for electroluminescence spectroscopy, all spectra (Figure 4c) were recorded above the Sn-Pc- u molecule. While the uu configuration of the dimer exceeds the spectral photon yield of the monomer by a factor of nearly 2, the ud configuration gives rise to a maximum spectral photon yield that falls below the monomer emission by a factor of almost 4, that is, the maximum spectral photon yields of the uu and ud dimer are more than a factor 6 apart. Additionally, spectroscopic fine structure is hardly observed in the emission spectrum of the ud dimer. Rather, the shape of the ud dimer spectrum resembles the broad background of the monomer spectrum with an indentation at the position of the monomer principal $S_1 \rightarrow S_0$ emission. The sharper feature at 1.76 eV may be due to the dipole-coupled $\uparrow\uparrow$ exciton mode of the TDC model (Figure 4d).

The remainder of this article is devoted to the tentative explanation of the markedly different photon yield of the uu and ud Sn-Pc dimers. The strong amplification of electroluminescence of the uu dimer relative to the u monomer is reminiscent of superradiance, which describes a cooperative optical effect that results from the radiative correlation of quantum emitters⁶⁶ provided by intermolecular dipole-dipole coupling resulting in a quantum coherent collective state.^{66–68} Superradiance was reported for Zn-Pc oligomers with STML.⁴¹ In agreement with the findings reported here, with increasing length of the oligomer chain the photon yield was augmented, the width of the electroluminescence spectrum narrowed, and its centroid was redshifted. This effect was particularly obvious for the transition from the Zn-Pc monomer to the dimer.⁴¹ The TDC model used above for rationalizing the electroluminescence fine structure of the uu dimer corroborates the superradiance scenario in that the dipole-coupled $\uparrow\uparrow$ exciton state is strongly enhanced for the uu dimer compared to the monomer, which hints at the in-phase superposition of the \uparrow transition dipole moments of the two individual monomers. It is then tempting to associate the low photon yield of the ud dimer with a subradiant state. However, the transition dipole moments of Sn-Pc- d are

expected to be the same as for Sn-Pc-*u*, and their coupling in the *ud* dimer are unlikely to be altered compared to the *uu* dimer.^{52,54} Indeed, the molecular orbitals underlying the exciton are the HOMO and the LUMO at the periphery of the macrocycle, which is nearly unaffected by the configurational switch. The observed reduction in the photon yield of the *ud* dimer could possibly be caused by different emission characteristics of the Sn-Pc-*d* monomer in the following sense. First, while for Sn-Pc-*d* electroluminescence spectroscopy was experimentally not feasible (vide supra), indirect evidence for the suggested configurational changes in the emission characteristics are provided by a recent STML study of VO-Pc on NaCl-covered Au(111).⁶⁹ For the two molecular configurations defined by the O atom above and beneath the backbone of the adsorbed molecule, a difference in the principal emission peaks of ≈ 25 meV was shown. Second, a comparable difference was observed for the Q-exciton-associated electroluminescence of Pt-Pc (1.945 eV) and Zn-Pc (1.901 eV) on NaCl-covered Ag(111).⁷⁰ Upon forming a heterodimer out of these molecules, the dimer principal emission peak was strongly redshifted to 1.887 eV. A similar scenario could be applicable to the *ud* dimer in the present case, too.

In conclusion, luminescence of a molecular dimer of Sn-Pc on NaCl-covered Au(111) can be mastered by changing the configuration of one of the constituent monomers. The reversibility of the configurational switch allows to turn on and off the light emission at the single-molecule level. The bright optical state is possibly due to superradiance as inferred from the comparison of the monomer STML spectrum, which exhibits vibrational progression and hot luminescence, with the dimer spectral data whose spectroscopic fine structure is due to excitonic states resulting from the coherent coupling of the monomer transition dipole moments. The dark optical state is tentatively assigned to the redshifted principal emission caused by the presumably different emission characteristics of the bistable molecular configurations of the monomers. The presented findings exemplify the external control of quantum coherent processes, that is, the on-demand presence of bright and dark optical states, which may be particularly relevant to the nanotechnology of quantum light sources.

Methods

The experiments were performed with an STM operated in ultrahigh vacuum (10^{-9} Pa) and at low temperature (5 K). Surfaces of Au(111) were cleaned and prepared by Ar^+ ion bombardment and annealing. Clean NaCl (purity: $\geq 99\%$) was sublimated at a temperature of 890 K on clean Au(111) at room temperature. The NaCl flux was controlled by a quartz microbalance. After NaCl deposition for 100 s, the covered sample was annealed at 470 K to yield a 50% coverage of 3 to 4 atomic layers with of NaCl. The solid phase of Sn-Pc molecules was sublimated from a ceramics crucible heated at 780 K. A coverage of approximately 20 Sn-Pc molecules per $80\text{ nm} \times 80\text{ nm}$ was achieved after deposition for 2 min onto the cold (6 K) NaCl-covered sample surface. A chemically edged and subsequently Ar^+ -bombarded Ag wire served as the tip material. Field emission on and repeated indentations into the clean Au surface presumably led to the coating of the tip apex with substrate material. Single-atom transfer from the tip to the sample gave rise to particularly sharp and stable probes.⁷¹⁻⁷⁴ Images were acquired in the constant-current and constant-height mode with the bias voltage applied to the sample and were further processed with the with the Nanotec Electronics WSxM software.⁷⁵ Spectroscopy of dI/dV proceeded via the sinusoidal modulation (5 mV, 726 Hz) of the dc sample voltage and measuring the first harmonic of the ac current response of the tunneling junction with a lock-in amplifier. For electroluminescence spectroscopy, a pair of two lenses, one placed inside and the other outside of the vacuum recipient, collects the light emitted from the tunneling junction (Supporting Information, Figure S1). High-resolution (wide-range) optical spectra were recorded with an optical grating of 1200 (300) grooves per mm.

Associated Content

Supporting Information

Supporting Information is available free of charge on the ACS Publication website at DOI: [hyperlink DOI]

Electroluminescence detection and spectroscopy with a scanning tunneling microscope, electroluminescence data processing, analysis of the Sn-Pc-*u* monomer electrofluorescence, spectroscopy of Sn-Pc monomer and dimer orbitals, fabrication of dimers and control of configurational molecular states, dependence of the dimer emission on the mutual monomer separation, adsorption of Sn-Pc on ultrathin NaCl films (PDF)

Data availability statement

The data that support the findings of this article are not publicly available upon publication because it is not technically feasible and/or the cost of preparing, depositing, and hosting the data would be prohibitive within the terms of this research project. The data are available from the authors upon reasonable request.

Author contributions

M.K. carried out the experiments and analyzed the data. M.K and J.K. wrote the manuscript. J.K. conceived the experiments. All authors discussed the data, their interpretation, and commented on the final version of the manuscript.

Acknowledgement

Funding by the German Federal Ministry of Education and Research within the "Forschungslabore Mikroelektronik Deutschland (ForLab)" initiative is acknowledged. Discussions with

Daniel Wegner on technical issues of light detection and with Lorenz Meyer, Marvin Kuß, Robert Henninger are appreciated.

References

- (1) Michler, P.; Imamoglu, A.; Mason, M. D.; Carson, P. J.; Strouse, G. F.; Buratto, S. K. Quantum correlation among photons from a single quantum dot at room temperature. *Nature* **2000**, *406*, 968–970.
- (2) Yuan, Z.; Kardynal, B. E.; Stevenson, R. M.; Shields, A. J.; Lobo, C. J.; Cooper, K.; Beattie, N. S.; Ritchie, D. A.; Pepper, M. Electrically Driven Single-Photon Source. *Science* **2002**, *295*, 102–105.
- (3) Santori, C.; Fattal, D.; Vučković, J.; Solomon, G. S.; Yamamoto, Y. Indistinguishable photons from a single-photon device. *Nature* **2002**, *419*, 594–597.
- (4) Kimble, H. J.; Dagenais, M.; Mandel, L. Photon Antibunching in Resonance Fluorescence. *Phys. Rev. Lett.* **1977**, *39*, 691–695.
- (5) Kuhn, A.; Henrich, M.; Rempe, G. Deterministic Single-Photon Source for Distributed Quantum Networking. *Phys. Rev. Lett.* **2002**, *89*, 067901.
- (6) Brouri, R.; Beveratos, A.; Poizat, J.-P.; Grangier, P. Photon antibunching in the fluorescence of individual color centers in diamond. *Opt. Lett.* **2000**, *25*, 1294–1296.
- (7) Mizuochi, N.; Makino, T.; Kato, H.; Takeuchi, D.; Ogura, M.; Okushi, H.; Nothaft, M.; Neumann, P.; Gali, A.; Jelezko, F.; Wrachtrup, J.; Yamasaki, S. Electrically driven single-photon source at room temperature in diamond. *Nature Photonics* **2012**, *6*, 299–303.
- (8) Iwasaki, T. et al. Germanium-Vacancy Single Color Centers in Diamond. *Scientific Reports* **2015**, *5*, 12882.

- (9) Basché, T.; Moerner, W. E.; Orrit, M.; Talon, H. Photon antibunching in the fluorescence of a single dye molecule trapped in a solid. *Phys. Rev. Lett.* **1992**, *69*, 1516–1519.
- (10) Lounis, B.; Moerner, W. E. Single photons on demand from a single molecule at room temperature. *Nature* **2000**, *407*, 491–493.
- (11) Kiraz, A.; Ehrl, M.; Hellerer, T.; Müstecaplıođlu, O. E.; Bräuchle, C.; Zumbusch, A. Indistinguishable Photons from a Single Molecule. *Phys. Rev. Lett.* **2005**, *94*, 223602.
- (12) Lettow, R.; Rezus, Y. L. A.; Renn, A.; Zumofen, G.; Ikonen, E.; Götzinger, S.; Sandoghdar, V. Quantum Interference of Tunably Indistinguishable Photons from Remote Organic Molecules. *Phys. Rev. Lett.* **2010**, *104*, 123605.
- (13) Nothaft, M.; Höhla, S.; Jelezko, F.; Frühauf, N.; Pflaum, J.; Wrachtrup, J. Electrically driven photon antibunching from a single molecule at room temperature. *Nature Communications* **2012**, *3*, 628.
- (14) Rezus, Y. L. A.; Walt, S. G.; Lettow, R.; Renn, A.; Zumofen, G.; Götzinger, S.; Sandoghdar, V. Single-Photon Spectroscopy of a Single Molecule. *Phys. Rev. Lett.* **2012**, *108*, 093601.
- (15) Bohnet, J. G.; Chen, Z.; Weiner, J. M.; Meiser, D.; Holland, M. J.; Thompson, J. K. A steady-state superradiant laser with less than one intracavity photon. *Nature* **2012**, *484*, 78–81.
- (16) Asenjo-Garcia, A.; Moreno-Cardoner, M.; Albrecht, A.; Kimble, H. J.; Chang, D. E. Exponential Improvement in Photon Storage Fidelities Using Subradiance and “Selective Radiance” in Atomic Arrays. *Phys. Rev. X* **2017**, *7*, 031024.
- (17) Facchinetti, G.; Jenkins, S. D.; Ruostekoski, J. Storing Light with Subradiant Correlations in Arrays of Atoms. *Phys. Rev. Lett.* **2016**, *117*, 243601.

- (18) Wild, D. S.; Shahmoon, E.; Yelin, S. F.; Lukin, M. D. Quantum Nonlinear Optics in Atomically Thin Materials. *Phys. Rev. Lett.* **2018**, *121*, 123606.
- (19) Guimond, P.-O.; Grankin, A.; Vasilyev, D. V.; Vermersch, B.; Zoller, P. Subradiant Bell States in Distant Atomic Arrays. *Phys. Rev. Lett.* **2019**, *122*, 093601.
- (20) Kimble, H. J. The quantum internet. *Nature* **2008**, *453*, 1023–1030.
- (21) Aharonovich, I.; Englund, D.; Toth, M. Solid-state single-photon emitters. *Nature Photonics* **2016**, *10*, 631–641.
- (22) Chan, M. L.; Bell, T. J.; Pettersson, L. A.; Chen, S. X.; Yard, P.; Sørensen, A. S.; Paesani, S. Tailoring Fusion-Based Photonic Quantum Computing Schemes to Quantum Emitters. *PRX Quantum* **2025**, *6*, 020304.
- (23) Aspuru-Guzik, A.; Walther, P. Photonic quantum simulators. *Nature Physics* **2012**, *8*, 285–291.
- (24) Barzanjeh, S.; Xuereb, A.; Gröblacher, S.; Paternostro, M.; Regal, C. A.; Weig, E. M. Optomechanics for quantum technologies. *Nature Physics* **2022**, *18*, 15–24.
- (25) Lombardi, P.; Trapuzzano, M.; Colautti, M.; Margheri, G.; Degiovanni, I. P.; López, M.; Kück, S.; Toninelli, C. A Molecule-Based Single-Photon Source Applied in Quantum Radiometry. *Advanced Quantum Technologies* **2020**, *3*, 1900083.
- (26) Zhang, Y.; Meng, Q.-S.; Zhang, L.; Luo, Y.; Yu, Y.-J.; Yang, B.; Zhang, Y.; Esteban, R.; Aizpurua, J.; Luo, Y.; Yang, J.-L.; Dong, Z.-C.; Hou, J. G. Sub-nanometre control of the coherent interaction between a single molecule and a plasmonic nanocavity. *Nature Communications* **2017**, *8*, 15225.
- (27) Imada, H.; Miwa, K.; Imai-Imada, M.; Kawahara, S.; Kimura, K.; Kim, Y. Single-Molecule Investigation of Energy Dynamics in a Coupled Plasmon-Exciton System. *Phys. Rev. Lett.* **2017**, *119*, 013901.

- (28) Kröger, J.; Doppagne, B.; Scheurer, F.; Schull, G. Fano Description of Single-Hydrocarbon Fluorescence Excited by a Scanning Tunneling Microscope. *Nano Letters* **2018**, *18*, 3407–3413.
- (29) Toninelli, C. et al. Single organic molecules for photonic quantum technologies. *Nature Materials* **2021**, *20*, 1615–1628.
- (30) Skribanowitz, N.; Herman, I. P.; MacGillivray, J. C.; Feld, M. S. Observation of Dicke Superradiance in Optically Pumped HF Gas. *Phys. Rev. Lett.* **1973**, *30*, 309–312.
- (31) Gross, M.; Fabre, C.; Pillet, P.; Haroche, S. Observation of Near-Infrared Dicke Superradiance on Cascading Transitions in Atomic Sodium. *Phys. Rev. Lett.* **1976**, *36*, 1035–1038.
- (32) Vrehen, Q. H. F.; Hikspoors, H. M. J.; Gibbs, H. M. Quantum Beats in Superfluorescence in Atomic Cesium. *Phys. Rev. Lett.* **1977**, *38*, 764–767.
- (33) DeVoe, R. G.; Brewer, R. G. Observation of Superradiant and Subradiant Spontaneous Emission of Two Trapped Ions. *Phys. Rev. Lett.* **1996**, *76*, 2049–2052.
- (34) Bopp, M. A.; Jia, Y.; Li, L.; Cogdell, R. J.; Hochstrasser, R. M. Fluorescence and photobleaching dynamics of single light-harvesting complexes. *Proceedings of the National Academy of Sciences* **1997**, *94*, 10630–10635.
- (35) Hettich, C.; Schmitt, C.; Zitzmann, J.; Kühn, S.; Gerhardt, I.; Sandoghdar, V. Nanometer Resolution and Coherent Optical Dipole Coupling of Two Individual Molecules. *Science* **2002**, *298*, 385–389.
- (36) Scheibner, M.; Schmidt, T.; Worschech, L.; Forchel, A.; Bacher, G.; Passow, T.; Hommel, D. Superradiance of quantum dots. *Nature Physics* **2007**, *3*, 106–110.
- (37) Zhang, Y.; Luo, Y.; Zhang, Y.; Yu, Y.-J.; Kuang, Y.-M.; Zhang, L.; Meng, Q.-S.;

- Luo, Y.; Yang, J.-L.; Dong, Z.-C.; Hou, J. G. Visualizing coherent intermolecular dipole-dipole coupling in real space. *Nature* **2016**, *531*, 623–627.
- (38) Araújo, M. O.; Krešić, I.; Kaiser, R.; Guerin, W. Superradiance in a Large and Dilute Cloud of Cold Atoms in the Linear-Optics Regime. *Phys. Rev. Lett.* **2016**, *117*, 073002.
- (39) Rainò, G.; Becker, M. A.; Bodnarchuk, M. I.; Mahrt, R. F.; Kovalenko, M. V.; Stöferle, T. Superfluorescence from lead halide perovskite quantum dot superlattices. *Nature* **2018**, *563*, 671–675.
- (40) Manna, B.; Nandi, A. Manifestation of Unforeseen Superradiance Phenomenon from Phenanthrene and Chrysene Nanoaggregates. *The Journal of Physical Chemistry C* **2019**, *123*, 21281–21289.
- (41) Luo, Y.; Chen, G.; Zhang, Y.; Zhang, L.; Yu, Y.; Kong, F.; Tian, X.; Zhang, Y.; Shan, C.; Luo, Y.; Yang, J.; Sandoghdar, V.; Dong, Z.; Hou, J. G. Electrically Driven Single-Photon Superradiance from Molecular Chains in a Plasmonic Nanocavity. *Phys. Rev. Lett.* **2019**, *122*, 233901.
- (42) Binnig, G.; Rohrer, H.; Gerber, C.; Weibel, E. Surface Studies by Scanning Tunneling Microscopy. *Phys. Rev. Lett.* **1982**, *49*, 57–61.
- (43) Becker, R. S.; Golovchenko, J. A.; Swartzentruber, B. S. Atomic-Scale Surface Modifications Using a Tunnelling Microscope. *Nature* **1987**, *325*, 419 – 421.
- (44) Eigler, D. M.; Schweizer, E. K. Positioning Single Atoms with a Scanning Tunnelling Microscope. *Nature* **1990**, *344*, 524 – 526.
- (45) Berndt, R.; Gaisch, R.; Gimzewski, J. K.; Reihl, B.; Schlittler, R. R.; Schneider, W. D.; Tschudy, M. Photon Emission at Molecular Resolution Induced by a Scanning Tunneling Microscope. *Science* **1993**, *262*, 1425–1427.

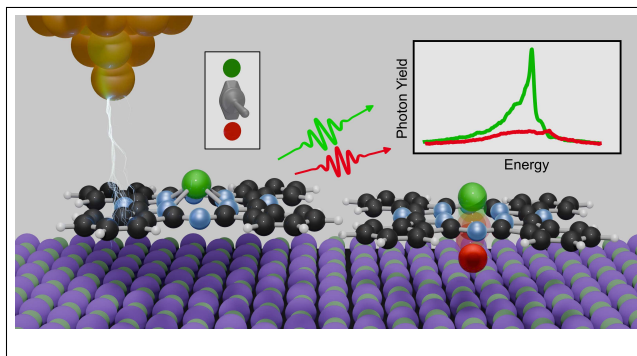
- (46) Qiu, X. H.; Nazin, G. V.; Ho, W. Vibrationally Resolved Fluorescence Excited with Submolecular Precision. *Science* **2003**, *299*, 542–546.
- (47) Rossel, F.; Pivetta, M.; Schneider, W.-D. Luminescence experiments on supported molecules with the scanning tunneling microscope. *Surface Science Reports* **2010**, *65*, 129 – 144.
- (48) Kuhnke, K.; Große, C.; Merino, P.; Kern, K. Atomic-Scale Imaging and Spectroscopy of Electroluminescence at Molecular Interfaces. *Chemical Reviews* **2017**, *117*, 5174–5222, PMID: 28294599.
- (49) Wang, Y.; Kröger, J.; Berndt, R.; Hofer, W. A. Pushing and Pulling a Sn Ion through an Adsorbed Phthalocyanine Molecule. *Journal of the American Chemical Society* **2009**, *131*, 3639–3643.
- (50) Lauwaet, K.; Schouteden, K.; Janssens, E.; Van Haesendonck, C.; Lievens, P. Dependence of the NaCl/Au(111) interface state on the thickness of the NaCl layer. *Journal of Physics: Condensed Matter* **2012**, *24*, 475507.
- (51) Wang, Y.; Kröger, J.; Berndt, R.; Hofer, W. Structural and Electronic Properties of Ultrathin Tin–Phthalocyanine Films on Ag(111) at the Single-Molecule Level. *Angewandte Chemie International Edition* **2009**, *48*, 1261–1265.
- (52) Gruenewald, M.; Peuker, J.; Meissner, M.; Sojka, F.; Forker, R.; Fritz, T. Impact of a molecular wetting layer on the structural and optical properties of tin(II)-phthalocyanine multilayers on Ag(111). *Phys. Rev. B* **2016**, *93*, 115418.
- (53) Forker, R.; Gruenewald, M.; Sojka, F.; Peuker, J.; Mueller, P.; Zwick, C.; Huempfer, T.; Meissner, M.; Fritz, T. Fraternal twins: distinction between PbPc and SnPc by their switching behaviour in a scanning tunnelling microscope. *Journal of Physics: Condensed Matter* **2019**, *31*, 134004.

- (54) Sumimoto, M.; Honda, T.; Kawashima, Y.; Hori, K.; Fujimoto, H. Theoretical and experimental investigation on the electronic properties of the shuttlecock shaped and the double-decker structured metal phthalocyanines, MPc and M(Pc)₂ (M = Sn and Pb). *Dalton Trans.* **2012**, *41*, 7141–7150.
- (55) Doležal, J.; Canola, S.; Hapala, P.; de Campos Ferreira; Cezar, R.; Merino, P.; Švec, M. Evidence of exciton-libron coupling in chirally adsorbed single molecules. *Nature Communications* **2022**, *13*, 6008.
- (56) Wu, S. W.; Nazin, G. V.; Ho, W. Intramolecular photon emission from a single molecule in a scanning tunneling microscope. *Phys. Rev. B* **2008**, *77*, 205430.
- (57) Chen, C.; Chu, P.; Bobisch, C. A.; Mills, D. L.; Ho, W. Viewing the Interior of a Single Molecule: Vibronically Resolved Photon Imaging at Submolecular Resolution. *Phys. Rev. Lett.* **2010**, *105*, 217402.
- (58) Reecht, G.; Scheurer, F.; Speisser, V.; Dappe, Y. J.; Mathevet, F.; Schull, G. Electroluminescence of a Polythiophene Molecular Wire Suspended between a Metallic Surface and the Tip of a Scanning Tunneling Microscope. *Phys. Rev. Lett.* **2014**, *112*, 047403.
- (59) Zhang, L.; Yu, Y.-J.; Chen, L.-G.; Luo, Y.; Yang, B.; Kong, F.-F.; Chen, G.; Zhang, Y.; Zhang, Q.; Luo, Y.; Yang, J.-L.; Dong, Z.-C.; Hou, J. Electrically driven single-photon emission from an isolated single molecule. *Nature Communications* **2017**, *8*, 580.
- (60) Torrente, I. F.; Franke, K. J.; Pascual, J. I. Spectroscopy of C₆₀ single molecules: the role of screening on energy level alignment. *Journal of Physics: Condensed Matter* **2008**, *20*, 184001.
- (61) Kasha, M.; Rawls, H. R.; El-Bayoumi, M. A. The exciton model in molecular spectroscopy. *Pure and Applied Chemistry* **1965**, *11*, 371–392.

- (62) Wang, Y.; Wu, K.; Kröger, J.; Berndt, R. Review Article: Structures of phthalocyanine molecules on surfaces studied by STM. *AIP Advances* **2012**, *2*, 041402.
- (63) Nacci, C.; Kanisawa, K.; Fölsch, S. Reversible switching of single tin phthalocyanine molecules on the InAs(111)A surface. *Journal of Physics: Condensed Matter* **2012**, *24*, 394004.
- (64) Schwarz, F.; Wang, Y. F.; Hofer, W. A.; Berndt, R.; Runge, E.; Kröger, J. Electronic and Vibrational States of Single Tin-Phthalocyanine Molecules in Double Layers on Ag(111). *The Journal of Physical Chemistry C* **2015**, *119*, 15716–15722.
- (65) Banerjee, A.; Ide, N.; Lu, Y.; Berndt, R.; Weismann, A. Adsorption-Site- and Orientation-Dependent Magnetism of a Molecular Switch on Pb(100). *ACS Nano* **2025**, *19*, 7231–7238.
- (66) Dicke, R. H. Coherence in Spontaneous Radiation Processes. *Phys. Rev.* **1954**, *93*, 99–110.
- (67) Scully, M. O.; Svidzinsky, A. A. The Super of Superradiance. *Science* **2009**, *325*, 1510–1511.
- (68) Tighineanu, P.; Daveau, R. S.; Lehmann, T. B.; Beere, H. E.; Ritchie, D. A.; Lodahl, P.; Stobbe, S. Single-Photon Superradiance from a Quantum Dot. *Phys. Rev. Lett.* **2016**, *116*, 163604.
- (69) Rai, V. N.; Holzer, C.; Rockstuhl, C.; Wulfhekel, W.; Gerhard, L. Gating upconversion electroluminescence in a single molecule via adsorption-induced interaction of unpaired spin. *arXiv* **2026**, *2508*, 11501.
- (70) Kong, F.-F.; Tian, X.-J.; Zhang, Y.; Zhang, Y.; Chen, G.; Yu, Y.-J.; Jing, S.-H.; Gao, H.-Y.; Luo, Y.; Yang, J.-L.; Dong, Z.-C.; Hou, J. G. Wavelike electronic en-

- ergy transfer in donor–acceptor molecular systems through quantum coherence. *Nature Nanotechnology* **2022**, *17*, 729–736.
- (71) Limot, L.; Kröger, J.; Berndt, R.; Garcia-Lekue, A.; Hofer, W. A. Atom Transfer and Single-Atom Contacts. *Phys. Rev. Lett.* **2005**, *94*, 126102.
- (72) Kröger, J.; Néel, N.; Limot, L. Contact to Single Atoms and Molecules with the Tip of a Scanning Tunneling Microscope. *J. Phys.: Condens. Matter* **2008**, *20*, 223001.
- (73) Néel, N.; Kröger, J.; Berndt, R. Quantized Conductance of a Single Magnetic Atom. *Phys. Rev. Lett.* **2009**, *102*, 086805.
- (74) Berndt, R.; Kröger, J.; Néel, N.; Schull, G. Controlled Single Atom and Single Molecule Contacts. *Phys. Chem. Chem. Phys.* **2010**, *12*, 1022–1032.
- (75) Horcas, I.; Fernández, R.; Gómez-Rodríguez, J. M.; Colchero, J.; Gómez-Herrero, J.; Baro, A. M. WSXM: A Software for Scanning Probe Microscopy and a Tool for Nanotechnology. *Rev. Sci. Instrum.* **2007**, *78*, 013705.

TOC Graphic



Supporting Information:

Configurational control of photon emission from a molecular dimer

Maximilian Kögler,* Nicolas Néel, and Jörg Kröger*

Institut für Physik, Technische Universität Ilmenau, D-98693 Ilmenau, Germany

E-mail: max.koegler@tu-ilmenau.de; joerg.kroeger@tu-ilmenau.de

Electroluminescence detection and spectroscopy with a scanning tunneling microscope

The experimental setup used in this work is illustrated in Figure S1. The focal point of lens 1 inside the vacuum recipient is the tunneling barrier between tip and sample. The collected and collimated light traverses a viewport of the chamber and is focused by lens 2 to an optical fiber. The fiber transports the light to the spectrometer. For wide range (high resolution) spectra, an optical reflection grating with 300 (1200) grooves per mm is used. The spatially dispersed light is detected by a charge-coupled device (CCD) camera, which is thermoelectrically cooled to 175 K.

Figure S1b shows a typical spectral photon yield distribution of the nanocavity plasmon (NCP) radiative decay recorded above a 3-layer NaCl island on Au(111). A strong increase of the photon yield is observed for energies exceeding 1.8 eV. The small plateau between 1.7 eV and 1.8 eV marks the energy window of interest in the present studies. Below 1.7 eV, the light due to the NCP is essentially quenched.

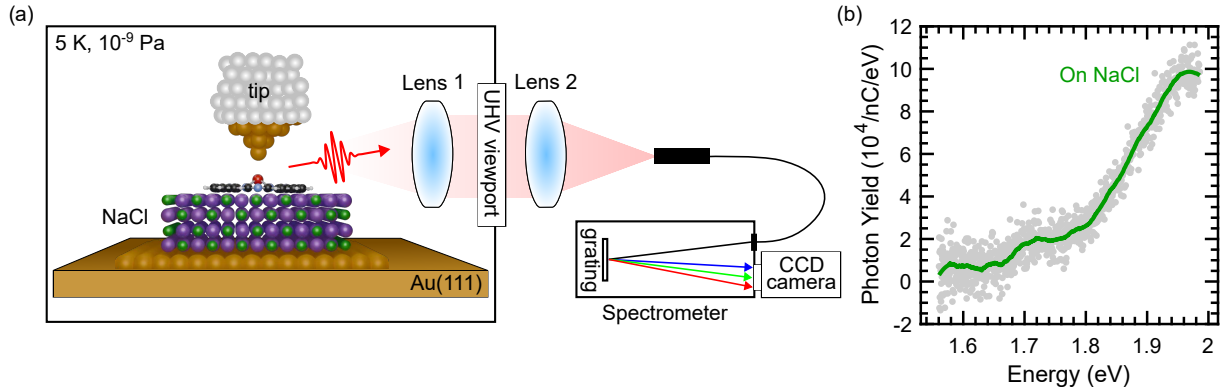


Figure S1: Experimental setup for STML and spectroscopy of the tip-induced plasmon radiation. (a) Sketch illustrating the setup for luminescence spectroscopy with an STM. (b) Spectral photon yield of the NCP radiative decay above 3 atomic layers of NaCl on Au(111) (2.5 V, 20 pA, 180 s).

Electroluminescence data processing

To understand the data processing it is useful to look at the photon emission mechanism in STML (Figure S2a). The quantum emitter is excited by charge injection, which gives rise to a molecular exciton that radiatively decays into a photon. The tip-induced plasmon or the NCP represents an important ingredient for the photon emission. It represents a collective charge oscillation in tip and sample, that is, a localized surface plasmon, which interacts with the tunneling electrons.^{S1-S3} The light emission spectrum depicted in Figure S1b can be viewed as a map of the available plasmonic modes of the nanocavity. The NCP density of states (DOS) at a specific energy determines the transition efficiency of an exciton with the same energy.^{S4,S5} Consequently, the NCP DOS can be viewed as an energy-dependent amplification factor for the exciton decay. It is noteworthy that the tip-induced breaking of the in-plane momentum conservation is a necessary condition for the coupling of NCP and the photon.

The red solid line in Figure S2b shows the raw NCP-associated luminescence obtained above 4 atomic layers of NaCl on Au(111). In the measured energy range, the NCP-related light signal is featureless, that is, it does not add any fine structure to the measured STML

spectra above Sn-Pc. To retrieve the genuine emission characteristics of the probed Sn-Pc-*u* molecule, the electrofluorescence spectrum acquired above the molecule must be normalized by the NCP luminescence. First, the background of the CCD camera must be removed (Figure S2b). Second, the raw STML signal, which gives the number of counts per CCD pixel (px), is translated into the physical unit (Figure S2c). To this end, the number of counts per CCD bin is divided by the associated energy interval and by the charge $I\tau$ (τ : exposure time of the CCD array) transported across the tunneling junction. Third, the electroluminescence data measured above the molecule is divided by the Savitzky-Golay-smoothed NCP spectral photon yield (Figure S2d).

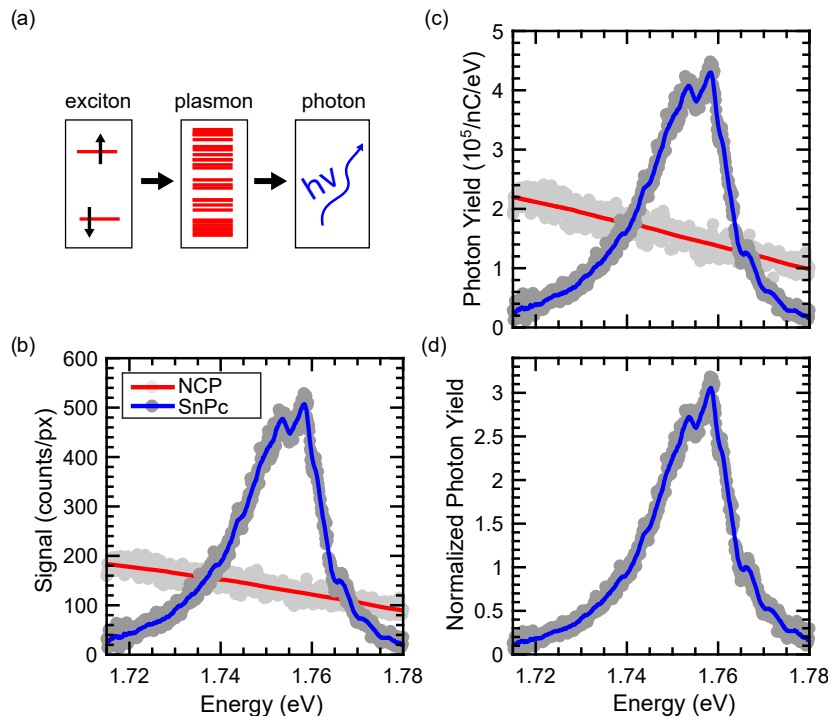


Figure S2: Principles underlying the STML data processing. (a) Sketch illustrating the radiative decay of a molecular exciton via the continuum of NCP modes. (b) Raw STML data acquired above an isoindole moiety of an Sn-Pc-*u* molecule (dark gray dots) above 4 atomic layers of NaCl on Au(111) (1.9 V, 50 pA, 240 s) together with STML data of the NCP (light gray dots) above the pristine NaCl island (1.9 V, 50 pA, 180 s), both corrected for the CCD background. Solid lines are smoothed data. (c) Same as (b) using physical units. (d) Result of dividing the molecular by the NCP luminescence spectrum.

Analysis of the Sn-Pc-*u* monomer electrofluorescence

Figure S3 investigates the Sn-Pc-*u* emission in detail. The visible spectroscopic fine structure is assigned to vibronic transitions. Each of them represents the relaxation from the vibrational state ν' of the excited electronic state S_1 to the vibrational state ν of S_0 (insets to Figures S3a,b). Within the Franck-Condon picture, the individual peak heights are defined by $|\langle \chi_\nu | \chi_{\nu'} \rangle|^2$ ($\chi_\nu, \chi_{\nu'}$: wave functions of vibrational states ν, ν') weighted by the occupation $p_{\nu'}$ of level ν' . Close to the vibrational equilibrium coordinates $R_0^{(\text{eq})}$ and $R_1^{(\text{eq})}$, the harmonic potentials $V_j \propto k_j \cdot [R - R_j^{(\text{eq})}]^2$ ($j = 0, 1$) with the generalized coordinate R describe well the potential landscape for vibrations in the electronic states S_0 and S_1 . Generally speaking, the vibrational potentials for S_0 and S_1 do not necessarily have the same curvature. For example, the restoring forces, which in the harmonic approximation are proportional to k_j , for frustrated rotations of metal-phthalocyanines on a NaCl substrate were demonstrated to differ for the electronic ground and excited state.^{S6}

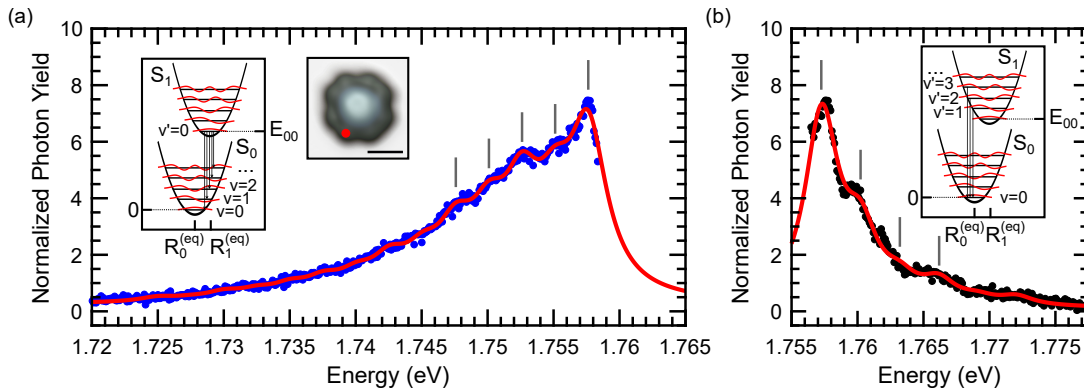


Figure S3: Line shape analysis of the Sn-Pc-*u* photon yield spectrum. (a) Low-energy ($E \leq E_{00}$) side of STML spectrum (dots) measured with the tip placed above an isoindole moiety of Sn-Pc-*u* (1.95 V, 50 pA, 180 s). The spectrum is normalized by the NCP electroluminescence spectrum (1.9 V, 50 pA, 120 s) above bare NaCl. The solid line represents a fit to the data with equidistantly spaced Lorentzians and identical width. Insets: illustration of vibrational progression (left) and constant-height current map of Sn-Pc-*u* (right, 1.9 V, the gray scale encodes currents ranging from 10 (dark) to 100 pA (bright), scale bar: 1 nm). (b) As (a) for high-energy ($E \geq E_{00}$) side of the STML spectrum. Inset: illustration of $S_1 \rightarrow S_0$ transitions for hot luminescence.

In the case $R_0^{(\text{eq})} \approx R_1^{(\text{eq})}$ and $k_0 \approx k_1$, the Franck-Condon factor prefers transitions with $\nu = \nu'$. According to Kasha's rule,^{S7} emission occurs predominantly from the $\nu' = 0$ level of S_1 . Therefore, the strongest photon yield observed at 1.758 eV (Figures S3a,b) is attributed to the principal transition between the vibrational ground states of S_0 and S_1 with energy $E_{\nu\nu'} = E_{00}$. The low-energy tail ($E \leq E_{00}$) of the luminescence spectrum (Figure S3a) contains the transitions from $\nu' = 0$ to $\nu > \nu'$ with an energy separation given by the vibrational energy quantum ε_0 of S_0 .

Matching the low-energy tail of the Sn-Pc-*u* principal emission peak with a superposition of Lorentzians with equidistant energy spacing (solid line in Figure S3a) allows to extract ε_0 . The broadening of the emission peaks due to transitions from $\nu' > 0$ as well as due to the finite lifetime of S_1 and experimental resolution is accounted for by a finite Lorentzian width, which is chosen identical for all Lorentzians in the fit. As a result of the fit, $\varepsilon_0 = 2.51 \pm 0.03$ meV. The uncertainty margin reflects the 95 % confidence interval of the fit parameter ε_0 underlying the least-squares fit to the electrofluorescence spectrum.

For the emission fine structure in the high-energy tail of the Sn-Pc-*u* principal transition, vibrational excited state of S_1 ($\nu' > 0$) have to be considered (inset to Figure S3b). The underlying hot luminescence requires $p_{\nu'} \neq 0$ for $\nu' > 0$. Apparently, direct tunneling into excited vibrational states and the enhanced radiative decay rate due to the NCP violates Kasha's rule,^{S7} as reported previously.^{S5,S6,S8,S9} The empirical Kasha rule^{S7} forbids molecular luminescence due to nonthermalized excitons. However, the fluorescence lifetime in a plasmonic environment can significantly be reduced and become comparable with the vibrational relaxation time in an electronic state. Therefore, luminescence peaks blueshifted from the principal $S_1(\nu' = 0) \rightarrow S_0(\nu = 0)$ transition can indeed occur. The energy spacing for the hot luminescence features is determined by ε_1 of S_1 , which again results from a fit to the data using a superposition of Lorentzians (solid line in Figure S2b) as $\varepsilon_1 = 2.96 \pm 0.07$ meV.

Because of the presence of hot luminescence, $p_{\nu'} \neq 0$ for $\nu' \geq 1$. Therefore, vibrational progression can occur from these vibrationally excited states of S_1 , too, which leads to a

broadening of the vibrational progression peaks in the series with $\nu' = 0$. For example, the vibrational progression transition $S_1(\nu' = 1) \rightarrow S_0(\nu = 2)$ exhibits the energy $E_{21} = E_{10} + \varepsilon_1 - \varepsilon_0$, which is very close to the $S_1(\nu' = 0) \rightarrow S_0(\nu = 1)$ transition with energy E_{10} .

Spectroscopy of Sn-Pc monomer and dimer orbitals

Figure S4 shows spectra of dI/dV obtained from Sn-Pc-*u* monomers and dimers. The wide-range spectrum in Figure S4a was acquired above the center of Sn-Pc-*u* on a 3-layer NaCl island. The onsets of peaks at negative (V_H) and positive (V_L) voltage (dotted lines in Figure S4a) are related to the HOMO and LUMO of Sn-Pc-*u*, respectively. To estimate the orbital energies E_H (HOMO) and E_L (LUMO), the voltage drop across the vacuum barrier (δV) and across the NaCl film ($(1 - \delta)V$) must be considered (Figure S4b) as well as the difference between the HOMO (LUMO) and the measured positive (negative) ion resonance.^{S10} In the following, both effects are combined in a single factor δ^* , i. e., $E_H = \delta^*eV_H$ and $E_L = \delta^*eV_L$ (e : elementary charge), which is in accordance with previous reports.^{S11-S14} For Sn-Pc-*u* on a 3-layer NaCl island, $V_H = -1.40$ V and $V_L = 1.52$ V (Figure S4a). The principal $S_1 \rightarrow S_0$ transition of Sn-Pc-*u* on a 3-layer NaCl island is observed at the energy $E_{00} = 1.76$ eV (not shown). Assuming now that the HOMO-LUMO gap approximately equals the Q-exciton energy,^{S14,S15} i. e., $E_{00} \approx E_L - E_H = \delta^*e(V_L - V_H)$, yields $\delta^* = 0.60$, $E_L = 0.92$ eV, and $E_H = -0.84$ eV for Sn-Pc-*u* on a 3-layer NaCl island. For Sn-Pc-*u* on a 4-layer NaCl island the onset of the LUMO signature (vertically offset data in Figure S4a, recorded above an isoindole group) appears at $V_L = 1.63$ V for the same feedback loop parameters as in the case of the 3-layer NaCl island, which according to $E_L = \delta^*eV_L$ results in $\delta^* = 0.56$. The HOMO signature was not accessible on 4-layer NaCl due to junction instabilities at elevated negative voltages.

Figures 2b,e of the article show that the maximum total photon yield of Sn-Pc-*u* on a 4-layer NaCl island is reached at about $\hat{V} = 2$ V. With the estimated $\delta^* = 0.56$, the energy

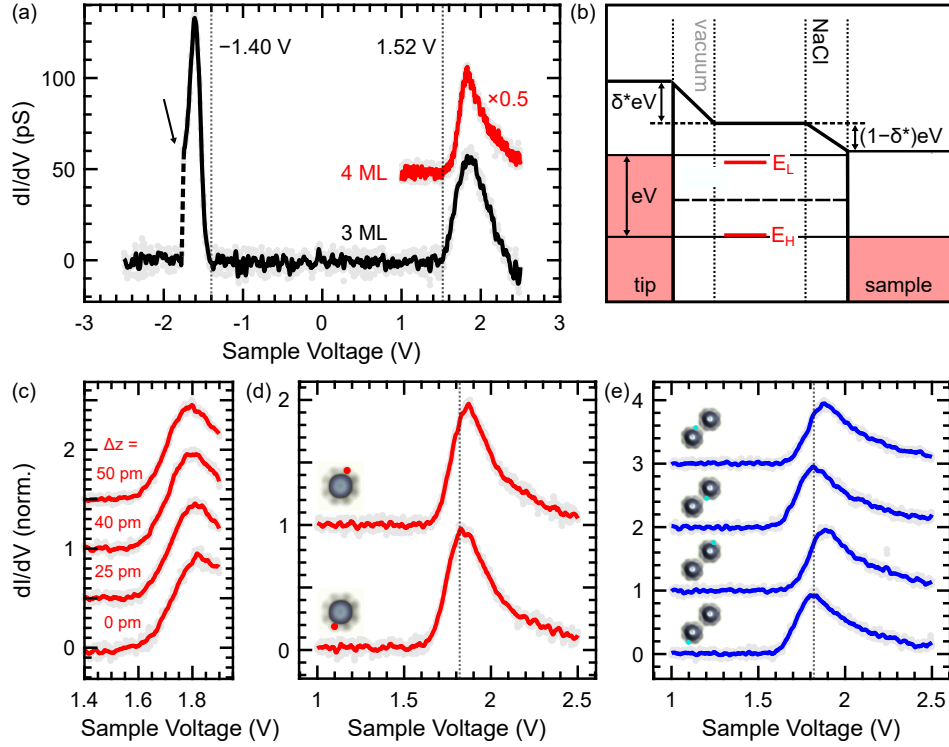


Figure S4: Spectroscopy of Sn-Pc-*u* monomer and dimer orbitals. (a) Wide-range spectrum (dots) of dI/dV of Sn-Pc-*u* on 3 atomic layers of NaCl on Au(111). The signature related to the HOMO (LUMO) appears as a peak with an onset at $V_H = -1.40$ V ($V_L = 1.52$ V). The black arrow marks the abrupt drop of the spectroscopic signal to 0 caused by the unintentional lateral displacement of the molecule. The LUMO feature of Sn-Pc-*u* adsorbed on a 4-layer NaCl island is vertically offset. Feedback loop parameters of both spectra: 1.9 V, 20 pA. (b) Illustration of the double tunneling barrier across the vacuum gap and the NaCl film (see text). (c) Dependence of the dI/dV LUMO-related signature on tip approach (from bottom to top). The feedback loop parameters 1.9 V, 20 pA define the tip displacement $\Delta z = 0$. (d) Dependence of the dI/dV LUMO-related signature (1.9 V, 20 pA) on the intramolecular site. The dashed line marks the peak position of the lower spectrum. Insets: constant-height current maps of the Sn-Pc-*u* monomer with indicated spectroscopy sites. (e) Same as (d) for an *uu* dimer. In (c)–(d), the spectra are normalized to their respective maximum and are vertically offset.

level alignment for the optimal photon yield can be derived. The chemical potential of the tip exhibits the energy distance $\delta^*e\hat{V} - E_L = 0.2 \text{ eV}$ above the LUMO level, while the chemical potential of the sample is $E_H - (1 - \delta^*)e\hat{V} = 0.06 \text{ eV}$ above the HOMO level. This level alignment at \hat{V} is schematically depicted in Figure S4b.

Figure S4c depicts the dependence of the LUMO-associated dI/dV spectrum of Sn-Pc-*u* on the tip approach by Δz to the center of an isoindole moiety. Due to the voltage drop across the vacuum barrier, a shift of the LUMO-related signature to higher voltages would be expected. However, the signature shifts to lower voltages by about 30 mV. Possibly, the voltage drop is overcompensated by the Stark effect^{S16,S17} the orbital is subject to in the electric field between the tip and the sample. The LUMO-related dI/dV signal likewise shows little variation ($< 100 \text{ meV}$) across different lobes both for the monomer and the dimer (Figures S4d,e), which is tentatively assigned to local electrostatic variations of the underlying ionic NaCl lattice. Supported by the unaltered emission spectra across all lobes of the monomer this small variation in the LUMO energy is irrelevant for the light emission of Sn-Pc-*u* monomers and dimers.

Fabrication of dimers and control of configurational molecular states

Two separated Sn-Pc-*u* molecules (Figure S5a) are pushed toward each other by placing the tip atop an isoindole group with feedback loop parameters -3.1 V and 20 pA . A successful pushing event of the molecule is reflected by a sudden current drop. A subsequent STM image of the same area (Figure S5b) shows the manipulated molecule which during the manipulation process switched to Sn-Pc-*d*. The $d \rightarrow u$ conversion is achieved by placing the tip above the Sn atom at positive sample voltage (1.9 V) with enabled feedback loop. Gradually increasing the tunneling current reliably leads to a sudden increase of the tip-sample distance, which signals the changed position of the Sn atom (Figure S5c). The dimer

fabrication is completed by executing another pushing cycle to decrease the mutual distance (Figure S5d).

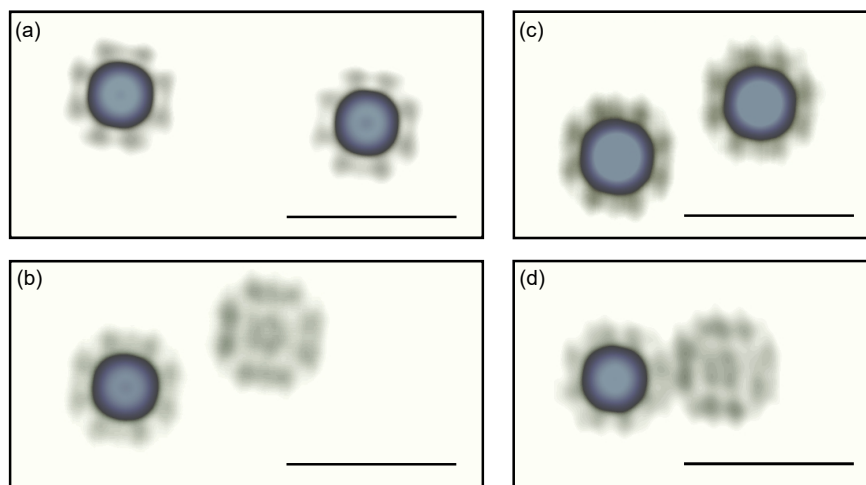


Figure S5: Lateral and configurational manipulation of Sn-Pc. (a) Constant-height current map of two separated Sn-Pc-*u* molecules on 4 atomic layers of NaCl (1.9 V, the gray scale encodes currents ranging from 2 (white) to 30 pA (gray)). (b) Same as (a) after the first lateral manipulation step applied to the right Sn-Pc-*u* in (a). A $u \rightarrow d$ conversion occurred to the manipulated Sn-Pc. (c) Same as (a) after conversion of the right Sn-Pc-*d* in (b) back to Sn-Pc-*u*. (d) As (a) after the second lateral manipulation step applied to the right Sn-Pc-*u* in (c). The scale bar in (a)–(d) depicts 3 nm.

The $u \rightarrow d$ conversion can be induced without moving the molecule when the tip is parked above the center of the molecule. After deactivating the feedback loop at 1.9 V, 5 pA the tip is retracted 60 pm. By gradually decreasing the sample voltage to ≈ -2.7 V gives rise to a sudden current drop, which signals successful conversion of Sn-Pc-*u* to Sn-Pc-*d*.

Dependence of the dimer emission on the mutual monomer separation

The uu dimer luminescence spectrum exhibits an overall redshift as a function of the separation of its constituent monomers (Figure S6). According to the point-dipole approximation this observation agrees well with expectations because $J_0 \propto 1/r^3$ (see article text). It is

noteworthy in this context that for dimers with similar center-to-center distances of the monomers, the actual geometry of the monomer-monomer hybridization is important. The split lobes of the monomers can be interlocked, that is, a lobe of one monomer is positioned between two adjacent lobes of the other monomer (Figure S6a). In another configuration the lobes overlap (Figure S6b). The two bottom luminescence spectra of Figure S6d show that the overlap configuration gives rise to a redshift of photon energies compared to the interlock configuration of the *uu* dimer.

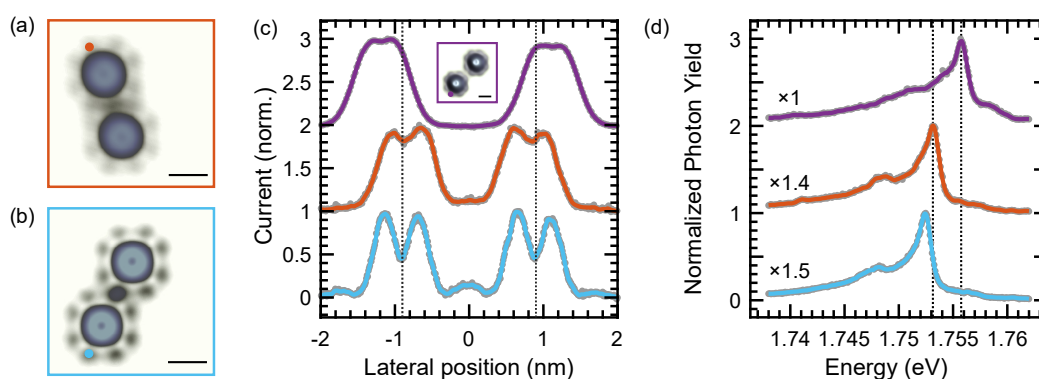


Figure S6: Dependence of the Sn-Pc-*u* dimer emission on the mutual monomer separation. (a) Constant-height STM image of an *uu* dimer with center-to-center distance of monomers of 1.7 nm (1.9 V, the gray scale encodes currents between 1.5 (dark) and 30 pA (bright)). (b) Constant-height STM image of an *uu* dimer with center-to-center distance of monomers of 1.8 nm (1.9 V, the gray scale encodes currents between 1.5 (dark) and 30 pA (bright)). (c) Cross-sectional profiles of constant-height current maps acquired atop *uu* dimers along a line connecting the molecular centers with mutual distances of 2.3 nm (top), 1.7 nm (middle), 1.8 nm (bottom). (d) Comparison of normalized photon yield (1.9 V, 50 pA, 240 s (top); 1.9 V, 50 pA, 180 s (middle); 1.9 V, 50 pA, 180 s (bottom)) of the *uu* dimers in (c). The spectra are normalized by the NCP luminescence spectrum acquired atop bare NaCl as well as to their respective maximum and are vertically offset. In (a),(b) and the inset to (c) the scale bar depicts 1 nm.

Adsorption of Sn-Pc on ultrathin NaCl films

For Sn-Pc-*u* on a 4-layer NaCl island (Figure S7a) the closely neighboring NaCl lattice was imaged with atomic resolution (Figure S7b). Extending the position of Cl ions, which are

clearly discerned as circular protrusions,^{S14,S18–S20} to the Sn-Pc-*u* adsorption site allows to analyze the adsorption site in more detail. The Sn atom adsorbs on a bridge site between two Cl ions, while the lobes point along the NaCl compact directions [001] and [010]. The lobes at the periphery of the isoindole groups cover inequivalent areas of the NaCl lattice.

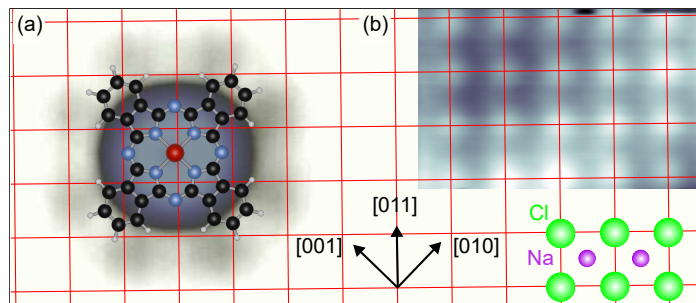


Figure S7: Adsorption of Sn-Pc-*U* on NaCl. (a) Constant-height STM image of an Sn-Pc-*u* adsorbed on a 4-layer NaCl island (1.9 V, the gray scale encodes currents between 2 pA (dark) and 40 pA (bright)). The superimposed molecule model reflects the relaxed Sn-Pc vacuum structure. (b) Constant-current STM image of the nearby NaCl lattice (1.9 V, 35 pA, the NaCl lattice has a corrugation of 4 pm). The grid lines intersect at the centers of Cl ions (circular protrusions). Compact directions ([010], [001], [011]) and a sketch of the NaCl lattice are shown.

References

- (S1) Rendell, R. W.; Scalapino, D. J.; Mühlischlegel, B. Role of Local Plasmon Modes in Light Emission from Small-particle Tunnel Junctions. *Phys. Rev. Lett.* **1978**, *41*, 1746–1750.
- (S2) Rossel, F.; Pivetta, M.; Schneider, W.-D. Luminescence experiments on supported molecules with the scanning tunneling microscope. *Surface Science Reports* **2010**, *65*, 129 – 144.
- (S3) Persson, B. N. J.; Baratoff, A. Theory of photon emission in electron tunneling to metallic particles. *Phys. Rev. Lett.* **1992**, *68*, 3224–3227.

- (S4) Doppagne, B.; Chong, M. C.; Bulou, H.; Boeglin, A.; Scheurer, F.; Schull, G. Electrofluorochromism at the single-molecule level. *Science* **2018**, *361*, 251–255.
- (S5) Kröger, J.; Doppagne, B.; Scheurer, F.; Schull, G. Fano Description of Single-Hydrocarbon Fluorescence Excited by a Scanning Tunneling Microscope. *Nano Letters* **2018**, *18*, 3407–3413.
- (S6) Doležal, J.; Canola, S.; Hapala, P.; de Campos Ferreira; Cezar, R.; Merino, P.; Švec, M. Evidence of exciton-libron coupling in chirally adsorbed single molecules. *Nature Communications* **2022**, *13*, 6008.
- (S7) Kasha, M. Characterization of electronic transitions in complex molecules. *Discuss. Faraday Soc.* **1950**, *9*, 14–19.
- (S8) Chong, M. C.; Sosa-Vargas, L.; Bulou, H.; Boeglin, A.; Scheurer, F.; Mathevet, F.; Schull, G. Ordinary and Hot Electroluminescence from Single-Molecule Devices: Controlling the Emission Color by Chemical Engineering. *Nano Letters* **2016**, *16*, 6480–6484, PMID: 27652517.
- (S9) Martín-Jiménez, A.; Lauwaet, K.; Jover, Ó.; Granados, D.; Arnau, A.; Silkin, V. M.; Miranda, R.; Otero, R. Electronic Temperature and Two-Electron Processes in Overbias Plasmonic Emission from Tunnel Junctions. *Nano Letters* **2021**, *21*, 7086–7092.
- (S10) Torrente, I. F.; Franke, K. J.; Pascual, J. I. Spectroscopy of C₆₀ single molecules: the role of screening on energy level alignment. *Journal of Physics: Condensed Matter* **2008**, *20*, 184001.
- (S11) Wu, S. W.; Nazin, G. V.; Chen, X.; Qiu, X. H.; Ho, W. Control of Relative Tunneling Rates in Single Molecule Bipolar Electron Transport. *Phys. Rev. Lett.* **2004**, *93*, 236802.

- (S12) Reecht, G.; Scheurer, F.; Speisser, V.; Dappe, Y. J.; Mathevet, F.; Schull, G. Electroluminescence of a Polythiophene Molecular Wire Suspended between a Metallic Surface and the Tip of a Scanning Tunneling Microscope. *Phys. Rev. Lett.* **2014**, *112*, 047403.
- (S13) Meng, Q.; Zhang, C.; Zhang, Y.; Zhang, Y.; Liao, Y.; Dong, Z. Tunneling electron induced molecular electroluminescence from individual porphyrin J-aggregates. *Applied Physics Letters* **2015**, *107*, 043103.
- (S14) Zhang, Y.; Luo, Y.; Zhang, Y.; Yu, Y.-J.; Kuang, Y.-M.; Zhang, L.; Meng, Q.-S.; Luo, Y.; Yang, J.-L.; Dong, Z.-C.; Hou, J. G. Visualizing coherent intermolecular dipole-dipole coupling in real space. *Nature* **2016**, *531*, 623–627.
- (S15) Kaiser, K.; Lieske, L.-A.; Repp, J.; Gross, L. Charge-state lifetimes of single molecules on few monolayers of NaCl. *Nature Communications* **2023**, *14*, 4988.
- (S16) Limot, L.; Maroutian, T.; Johansson, P.; Berndt, R. Surface-State Stark Shift in a Scanning Tunneling Microscope. *Phys. Rev. Lett.* **2003**, *91*, 196801.
- (S17) Kröger, J.; Limot, L.; Jensen, H.; Berndt, R.; Johansson, P. Stark effect in Au(111) and Cu(111) surface states. *Phys. Rev. B* **2004**, *70*, 033401.
- (S18) Hebenstreit, W.; Redinger, J.; Horozova, Z.; Schmid, M.; Podloucky, R.; Varga, P. Atomic resolution by STM on ultra-thin films of alkali halides: experiment and local density calculations. *Surface Science* **1999**, *424*, L321–L328.
- (S19) Lauwaet, K.; Schouteden, K.; Janssens, E.; Van Haesendonck, C.; Lievens, P. Dependence of the NaCl/Au(111) interface state on the thickness of the NaCl layer. *Journal of Physics: Condensed Matter* **2012**, *24*, 475507.
- (S20) Kaiser, K.; Gross, L.; Schulz, F. A Single-Molecule Chemical Reaction Studied by

High-Resolution Atomic Force Microscopy and Scanning Tunneling Microscopy Induced Light Emission. *ACS Nano* **2019**, *13*, 6947–6954.